2.3 FABRICATION AND CHARACTERIZATION OF FE–{100}YTO BILAYERS —T. Stan, Y. Wu, and G. R. Odette (University of California Santa Barbara), H. D. Zhou (University of Tennessee)

OBJECTIVE

The objective of this work is to fabricate surrogate bulk Fe:$Y_2Ti_2O_7$ interfaces in the form of bilayers that are amenable to detailed characterization techniques and irradiation experiments.

SUMMARY

Nanostructured Ferritic Alloys (NFAs) have a Fe-Cr matrix and are dispersion strengthened by < 5 nm Y-Ti-O nano-oxide (NO) phases. The interfaces between the Y-Ti-O NO, such as $Y_2Ti_2O_7$ (YTO), and the surrounding matrix provide many favorable characteristics pertinent to fusion environments, such as trapping He in fine-scale bubbles. As a supplement to current characterization efforts of the NOs themselves, surrogate bulk Fe-YTO interfaces have been fabricated by electron beam Fe deposition on {100} YTO substrates. Grains with the {110}Fe||{100}YTO and <111>Fe||<110>YTO orientation relationship (OR) matched the two-fold symmetry of the {100}YTO substrate. This OR is not observed in embedded NOs. These results will support the development of computational models to predict NFA behavior.

PROGRESS AND STATUS

Introduction

Materials for nuclear fusion applications must reliably perform at high temperatures and manage high levels of helium (He). Nanostructured Ferritic Alloys (NFAs) are a promising class of Fe-Cr-based stainless steels that have remarkable mechanical properties, are thermally stable up to 1000 °C, and are irradiation tolerant [1-3]. NFAs contain a high density (~$10^{23}/m^2$) of 2-3 nm Y-Ti-O nano-oxide (NO) which help impede dislocation climb and glide, stabilize dislocation and grain structures, and trap He in fine-scale bubbles at matrix-NO interfaces that prevent void swelling and He embrittlement. Indeed, NFAs may turn He from a liability to an asset. For example, He bubbles act as recombination sites for vacancies and interstitials, thus promoting self-healing. The high density of matrix-NO interface pinning sites prevents He from collecting at grain boundaries, which would otherwise degrade creep and fracture properties.

There is ongoing research to determine the compositions, structures, and matrix-NO orientation relationships (ORs) for the NOs. A summary of these studies and other NFA properties was recently published by Odette [1]. The most common reported NO is $Y_2Ti_2O_7$ (YTO) fcc pyrochlore. Characterization and analysis of the NO:matrix interfaces is needed to develop first-principles atomic interface models necessary for predicting NFA performance in fusion reactor environments. YTO-matrix orientation relationships (ORs) are of interest because they affect interface defect structures, misfit strains, and energies.

There is a difference between bulk ORs and interfacial ORs. Bulk ORs refer to the overall relationship between two crystal lattices. The nomenclature involves listing any two non-linearly related parallel planes and directions between the lattices. Interfacial ORs describe the specific planes that are touching at an interface. The nomenclature involves listing the specific plane names and at least one set of parallel directions. Thus, a NO particle has only one bulk OR with the matrix, but may have many different interfacial ORs depending on the particle shape. In many cases, the 2-3 nm NOs have been shown to be cuboidal with flat matrix-YTO interfaces [4-6].

Cube-on-cube [4,5] and edge-on-cube [4,6] bulk ORs have been reported for embedded NOs. Their associated interfacial ORs have been summarized in Table 1, and are referred to as OReA – OReF where e refers to embedded. A schematic of each interfacial OR is shown with the surface orientation pointing out of page. The cube-on-cube bulk OR has interfaces where both matrix and NO faces (OReA), edges (OReB), or corners (OReC) are touching. The cuboidal NOs with cube-on-cube bulk OR have predominantly OReA and OReB interfacial ORs, and very small areas with OReC. The edge-on-cube bulk

OR has interfaces where a cube face is touching another face, or an edge. Note that some NO edges were blurry in Dawson et al. [4]; thus, the OReE interface may actually have been OReD. The ORs observed in this study are also listed in Table 1 as ORd1 – ORd3 where d refers to deposited.

Table 1. Reported bulk orientation relationships (ORs) and associated interfacial ORs.

Name	Bulk OR	Interfacial OR	Schematic	Reference
OReA	**Cube on Cube**	$\{100\}_{Fe}$ || $\{100\}_{YTO}$ $<100>_{Fe}$ || $<100>_{YTO}$ $<110>_{Fe}$ || $<110>_{YTO}$	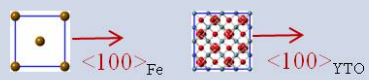	Dawson et al. Ribis et al.
OReB	**Cube on Cube**	$\{110\}_{Fe}$ || $\{110\}_{YTO}$ $<100>_{Fe}$ || $<100>_{YTO}$ $<110>_{Fe}$ || $<110>_{YTO}$	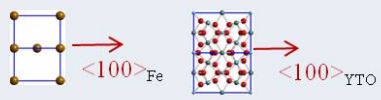	Dawson et al.
OReC	**Cube on Cube**	$\{111\}_{Fe}$ || $\{111\}_{YTO}$ $<110>_{Fe}$ || $<110>_{YTO}$	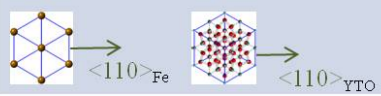	Dawson et al.*
OReD	*Cube on Edge*	$\{100\}_{Fe}$ || $\{100\}_{YTO}$ $<110>_{Fe}$ || $<100>_{YTO}$ $<100>_{Fe}$ || $<110>_{YTO}$	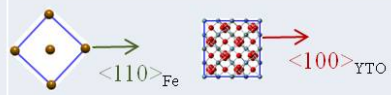	Dawson et al. Ciston et al.
OReE	*Cube on Edge*	$\{110\}_{Fe}$ || $\{100\}_{YTO}$ $<100>_{Fe}$ || $<100>_{YTO}$ $<110>_{Fe}$ || $<100>_{YTO}$	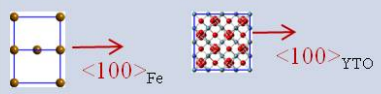	Dawson et al.**
OReF	*Cube on Edge*	$\{100\}_{Fe}$ || $\{110\}_{YTO}$ $<100>_{Fe}$ || $<100>_{YTO}$ $<100>_{Fe}$ || $<110>_{YTO}$	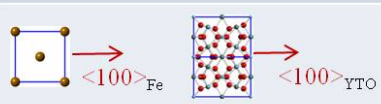	Ciston et al.
ORd1	**Edge on Corner**	$\{110\}_{Fe}$ || $\{111\}_{YTO}$ $<100>_{Fe}$ || $<110>_{YTO}$ $<110>_{Fe}$ || $<112>_{YTO}$	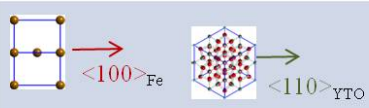	Fast Fe-{111}YTO
ORd2	*Cube on Corner*	$\{100\}_{Fe}$ || $\{111\}_{YTO}$ $<100>_{Fe}$ || $<110>_{YTO}$ $<100>_{Fe}$ || $<112>_{YTO}$	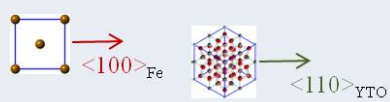	Slow Fe-{111}TYO 2-5 nm interfacial MO_x layer
ORd3	**Rotated Edge on Cube**	$\{110\}_{Fe}$ || $\{100\}_{YTO}$ $<112>_{Fe}$ || $<110>_{YTO}$ $<111>_{Fe}$ || $<110>_{YTO}$	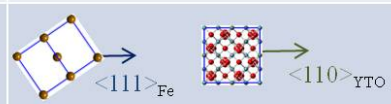	Fast Fe-{100}YTO

**The OReC interface is the least common. **The OReE interface may not actually be seen in NFAs.*

The nm-scale NOs are difficult to characterize using conventional microscopy techniques due to their small size. The research approach in this study is to deposit Fe on oriented YTO single crystal substrates to create surrogate mesoscopic-scale interfaces. These bilayers may or may not have similar interfacial characteristics to those found for embedded NO. Even if the bilayers do not have same characteristics as the embedded ones, this study will further the general understanding of metal-oxide interfaces. Surrogate interfaces are also amenable to irradiation studies such as interactions with point defects and He. Characterization of the Fe-YTO interfaces will help develop and improve first-principles atomic interface models, and help predict NFA performance.

Studies of Fe deposited on {111}YTO and {110}YTO were previously reported by Stan et al. [7] and in other Fusion Semiannual Reports [8,9]. This study is a continuation of the previous results by reporting depositions on {100}YTO single crystal substrates. The naturally selected interfaces are characterized and their implications to NOs in NFAs are discussed.

Experimental

The details of how samples were fabricated and the characterization instruments are covered in a previous publication [7]. In summary, YTO single crystals were {100} surface oriented and 2 mm thick wafers were cut using a wire saw. An Allied Multiprep instrument was used to polish the wafers using a sequence of diamond lapping films, followed by a final 15 minute polishing step using a 0.02 µm non-crystallizing colloidal silica suspension. Immediately after colloidal silica polishing and prior to Fe deposition, the substrates were placed under running water and gently scrubbed with Micro-Organic soap. This was followed by an acetone sonic bath for 10 minutes, and finally an isopropanol bath for 10 minutes.

An electron beam system was used to deposit Fe on the {100}YTO substrates at 800°C with a 10°C/min ramp up and down rate. While in the system and prior to Fe deposition, all of the substrates were left in vacuum at 800 ^{o}C for 1 hour. The deposition parameters are summarized in Table 2.

Table 2. Summary of deposition conditions.

Sample Name	Vacuum	Fe Thickness	Rate	Deposition time
Slow	8 x 10^{-6} torr	≈ 0.2 µm	0.3 nm/s	600 s
Fast	3 x 10^{-6} torr	≈ 2.0 µm	8.0 nm/s	250 s

Results

The following figures, each with parts a – g, show SEM and EBSD data that describe the depositions in this study. Part a is an SEM image or EBSD band contrast image showing grain size and shape. Part b shows EBSD inverse pole figure (IPF) maps depicting the out-of-plane crystallographic orientation of the Fe grains. Part c shows the same data as part b but represented as Euler pole figure (PF) maps indicating the full orientation of the Fe grains. In all figures, parts a – c show representative 10 µm by 10 µm areas such that the results can be easily compared for different depositions. Part d shows three PFs (<100>, <110> and <111> reflections) of the data shown in the maps of part a, colored according to the out-of-plane grain orientation (IPFZ). Part e shows three PFs of the Euler map in part c. Part f shows the substrate orientation as represented by PFs. Part g shows the 3D rendering of the Fe grains and substrate. The Fe-YTO ORs were obtained by overlapping spots in the Fe PFs with the accompanying YTO PFs.

<u>Slow Fe</u>

The first deposition was done using a slow rate of 0.3 nm/s to a total film thickness of 0.2 µm. The Fe grain size and topology are seen in Figures 1a-c. The grain size ranges from 0.5 – 2 µm, and the grains have an ~ 1:1 aspect ratio. Figure 1b is completely colored green indicating strong {110}Fe texturing. The Euler map in Figure 1c shows two dominant colors (blue and light orange) indicating two in-plane orientations of the Fe grains. The green areas in Figure 1c are believed to be mis-indexed portions of the blue grains.

The Fe PFs in Figures 1d–e have rings which usually imply a lack of in-plane orientation. However, the blue and light orange coloring indicates that there are two dominant orientations. The lack of distinct spots was previously believed to be caused by charging of the Fe film and misindexing of some grains. This effect was also present in later scans but removed for clarity. By overlapping select spots from the Fe PFs in Figure 1d with spots from the YTO PFs in Figure 1f, the following OR is obtained:

ORd3: {110}Fe || {100}YTO and <111>Fe || <110>YTO

This type of edge-on-cube orientation has not been observed for embedded NO in NFA. The 3D renderings in Figure 1g show that the Fe grains have a <111>Fe direction matched with one of the two <110>YTO in-plane directions. The blue and light orange grains have the exact same OR with the substrate, but are 90° rotated from one another and match the 2-fold symmetry of the underlying YTO.

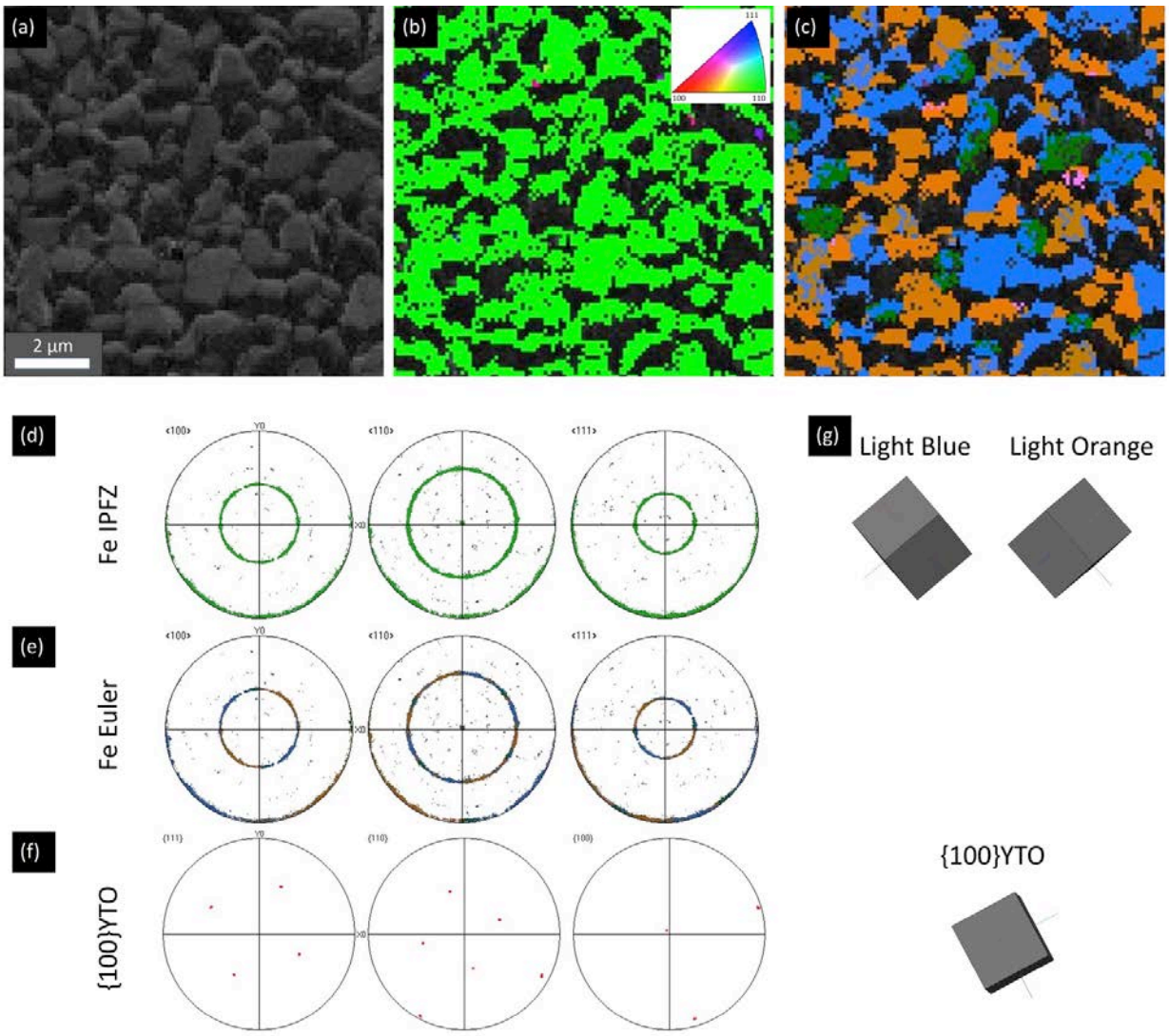

Figure 1. a) Band contrast, b) inverse PF map, and c) Euler map of the Fe film for the slow deposition. Fe PFs colored according to the d) out-of-plane orientation and e) Euler representation. f) YTO substrate PFs. g) 3D renderings of the Fe grains and YTO substrate.

Fast Fe

The previous deposition did not yield a large Fe film with a single dominant OR as desired. Thus the film was removed and the substrate was polished to have a new {100}YTO surface. The sample was cleaned and a thicker 2.0 µm film was deposited at a higher rate of 8 nm/s. A thicker film was chosen to ensure full coalescence of the Fe layer. A faster deposition was used to get a higher purity Fe film.

Figure 2a is an SEM image of the Fe film showing larger ~2 µm grains. Surface charging prevented large EBSD scans, thus smaller 6 µm by 6 µm data sets were collected. The EBSD data are shown in

Figures 2a–f and the results are consistent with the slow deposition. The rings in the PFs have been digitally removed and the dominant ORs are clearly visible as:

ORd3: {110}Fe || {100}YTO and <111>Fe || <110>YTO

The light blue and light orange grains are 90° rotated from each other and have only one OR with the substrate. This OR was not observed for embedded NOs.

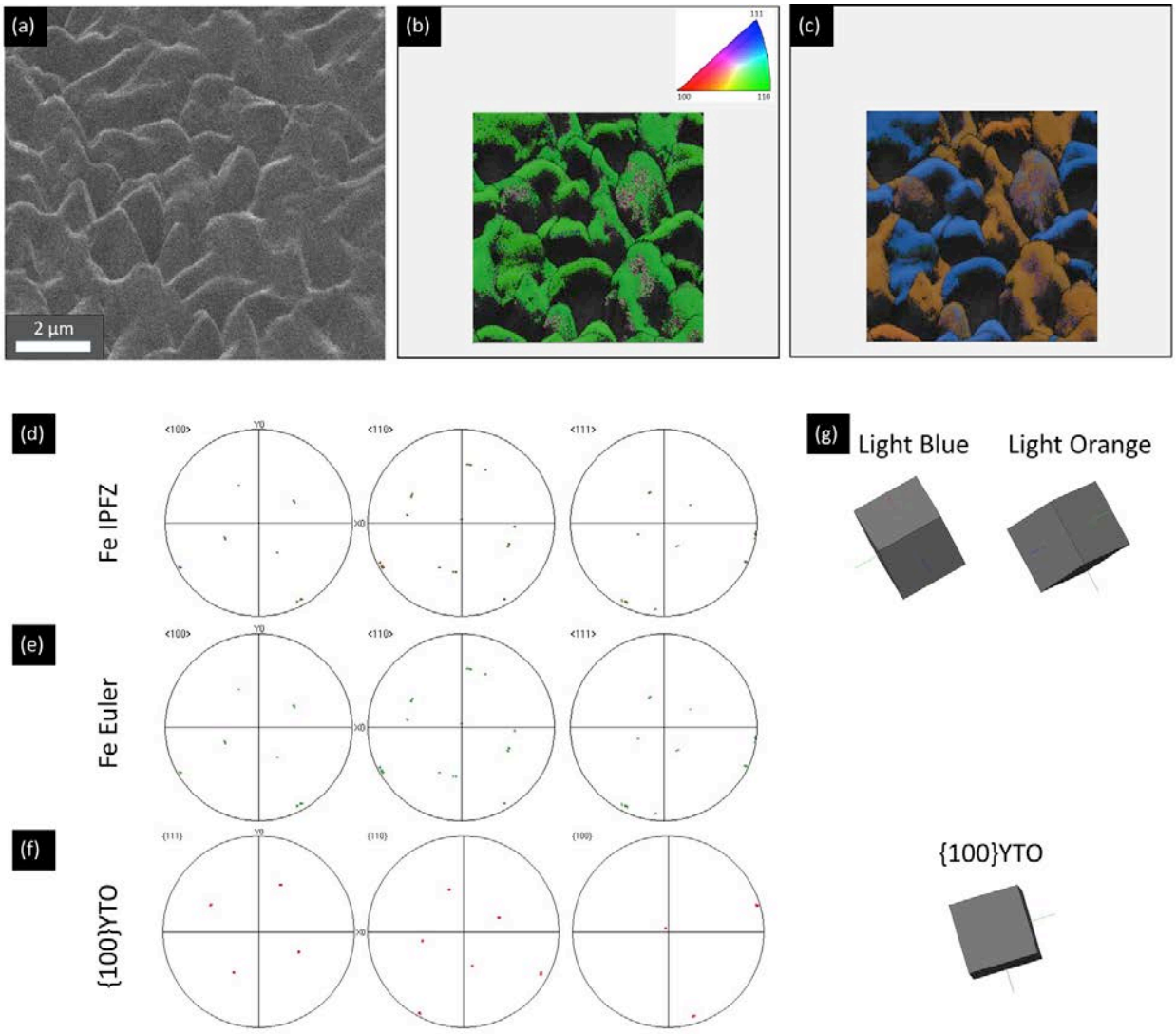

Figure 2. a) SEM image, b) inverse PF map, and c) Euler map of the Fe film for Area 1 of the fast deposition. Fe PFs colored according to the d) out-of-plane orientation and e) Euler representation. Note that the rings in the PFs were removed to isolate the dominant grain orientation. f) YTO substrate PFs. g) 3D renderings of the Fe grains and YTO substrate.

Discussion and Future Studies

The OR observed for the deposited film is {110}Fe||{100}YTO and <111>Fe||<110>YTO. Preliminary HRTEM and STEM data indicate that the grains have a relatively thick interlayer (~ 5 nm). This was

seen previously [7] where the presence and thickness of a metallic oxide interlayer directly affected the Fe grain orientation. Further, some areas of the two previously discussed films had areas with {110} textured Fe grains but no low-index in-plane matching. The cause of these areas will be investigated.

Three other depositions on {100}YTO were carried out, but the results were clearly affected by artifacts during the deposition. The Fe films had randomly oriented grains which are not useful for Fe-YTO studies. These films will be removed and the substrates will be re-polished. The e-beam system has been cleaned and repaired in preparation for future depositions.

Further, two depositions of Fe on amorphous silica substrates were carried out. The first used the Fe electron beam deposition system at a temperature of 800°C and ~10^{-6} torr as in previous studies. The Fe grains were mostly randomly oriented, with some grains exhibiting a {100}Fe texturing and random in-plane orientation. A similar experiment was done using an electron beam in a molecular beam epitaxy system at 100°C and ultrahigh vacuum of 10^{-10} torr. The two experiments yielded similar grain morphologies with mostly randomly oriented Fe grains and some {100} Fe texturing. These results are being analyzed in more detail.

The bilayers are being prepared for future He implantation and dual-beam irradiation studies. The results will help inform first-principle models of metallic oxide interfaces, as well as reaction-rate theory models for predicting NFA behavior.

References

[1] G. R. Odette, JOM. 66, 12, (2014) 2427
[2] G. R. Odette, M. J. Alinger, B. D. Wirth, Annu. Rev. Matter. Res. 38 (2008) 471
[3] Y. Dai, G. R. Odette, T. Yamamoto, Comp. Nuc. Mat. (2012) Elsevier
[4] K. Dawson, G. J. Tatlock, J. Nuc. Mat. 444 (2014) 252
[5] J. Ribis, Y. de Carlan, Acta Mat. 60 (2012) 238
[6] J. Ciston, Y. Wu, G. R. Odette, et al., Fus. Mat. Semiann. Prog. Rep. (2012) DOE-ER-0313/51
[7] T. Stan, Y. Wu, G. R. Odette, et al., Metal. and Mater. Trans. A, 44, 10 (2013) 4505
[8] T. Stan, Y. Wu, G. R. Odette, Fus. Semiann. 56 (2013) DOE-ER-0313/56
[9] T. Stan, Y. Wu, S. Kraemer, et al., Fus. Semiann. 57 (2014) DOE/ER-0313/57